*Asian Journal of Physics* Vol XX, Nos X-XX (2023) X-XX

# Sensitivity Analysis of a Double Corrugated Waveguide Slow Wave Structure for a 151 - 161.5 GHz TWT

Jeevan M. Rao, Rupa Basu, Rosa Letizia, Claudio Paoloni
*School of Engineering, Lancaster University, Lancaster, LA1 4YW, United Kingdom*
*Corresponding Author's email: c.paoloni@lancaster.ac.uk*

**Abstract:** TWTs at D-band (141 – 174.5 GHz) are the most promising solution to provide high transmission power for enabling long range wireless links with high capacity at sub-THz frequency. A D-band TWT was designed in the 151 - 161.5 GHz frequency band with about 10 W output power. The double corrugated waveguide is adopted as slow wave structure (SWS) for the relatively easy fabrication and alignment in comparison to other SWSs typically used at sub-THz frequency. Due to the short wavelength at D-band, the fabrication requires high precision CNC milling machining and tight tolerance control.

The sensitivity analysis of performance as a function of the dimensions of a device is an important method to predict in advance how the performance of are affected by geometry variations and the required level of fabrication accuracy to meet the specifications. It is also a useful tool to assist design to find the best initial dimensions for the final optimization.

This paper discusses the sensitivity analysis applied to the double corrugated waveguide (DCW) to be used in a 151 - 161.5 GHz TWT. A broad range of parameters are considered demonstrating the importance of fabrication accuracy and the eventual correction options for a correct functioning. The impact of fillets in the DCW pillars is also evaluated to eventually ease the fabrication requirement.

**Keywords:** Sub-THz, D-band, traveling wave tube, double corrugated waveguide, sensitivity analysis

## Foreword

This paper contains some unpublished work of Jeevan M Rao, research associate at Lancaster University, sadly passed away the 25th December 2020.

## 1. Introduction

The D-band with 27.5 GHz of available bandwidth allocated in three different frequency bands in the range 141 – 174.5 GHz is potentially able to support links with tens of Gigabits per second (Gb/s) [1 -3]. Numerous D-band front ends based on solid state power amplifiers (SSPAs) were reported with high data rate but the low power limited the transmission distance [3]. The high free space path loss and attenuation, especially in rain condition requires transmission power at Watt level, not available from SSPA, for satisfying the link budget.

Traveling wave tubes (TWTs) are the only amplifiers able to provide level of power in the range of 10s Watt at D-band [4 - 11]. TWTs at D-band are still state of the art devices. The only working TWTs presented in literature are based on the folded waveguide [8, 9]. The fabrication of the folded waveguide requires tight mechanical tolerances due to the high accuracy required to align the parts and their small dimensions.

A different approach is the use of the double corrugated waveguide (DCW) as slow wave structure at D-band [6, 12]. The DCW consists of two identical parallel rows of pillars to form a channel where the electron beam flows. When the two rows of pillars are sufficiently close together, they enhance the axial electric field in a quasi-circular shape to suitably interact with a circular electron beam. The fabrication approach is to fabricate the waveguide with the pillars in one block. A second block with a flat surface closes the waveguide, making the alignment of the two blocks simple. The assembly is completed by the diffusion bonding the two blocks together to form a robust structure from manufacturing point of view [6].

This paper discusses a sensitivity analysis of the variation of the different dimensions of the DCW, such DCW width, pillar height, period, electron beam position, important to assess the impact of the fabrication tolerance on the electrical behavior to predict possible performance variations.

## 2. D-band double corrugated waveguide design

A double corrugated waveguide has been designed in the band 151 - 161.5 GHz [11]. The single cell of the DCW is shown in Fig. 1. Figure 2 shows the cross section and the top view. The nominal dimensions are listed in Table I. The DCW is assumed to be used with 13.9 kV beam voltage. To note the very small pillar cross-section, 90 x 90 μm, due to the short wavelength at the operation frequency. These dimensions make the fabrication challenging and the tolerance requirements demanding.

A small variation of the dimensions from the nominal value could affect dispersion and interaction impedance with possible performance degradation in the operation band. A sensitivity analysis of the variation of main dimensions is important to ensure the correct DCW behavior and to define the fabrication requirements. The sensitivity analysis will

also permit to find possible mitigation solutions in case of deviation of performance from specifications, e.g. direction of variation of the beam voltage to compensate variations of the dispersion from the nominal one.
In the following, the sensitivity analysis on dispersion and interaction impedance as a function of the most critical dimensions such as the period *p*, the waveguide width *a*, the pillar height *b*, and beam position *d* and area section, will be discussed for the DCW with square pillars in Fig.1a.
The dispersion and the interaction impedance computed by using the nominal dimensions in Table 1are shown in Fig.3. The dispersion is almost flat in a wide band including the operation band ensuring the synchronism with the electron beam. The interaction impedance is slightly higher than 1 Ω over the full frequency band. At D-band this value of interaction impedance is suitable for achieving up to 10 W output power.
Figure 4 shows the dispersion curve with superimposed beam line at 13900 V. The wide overlap region provides very wide band behavior.

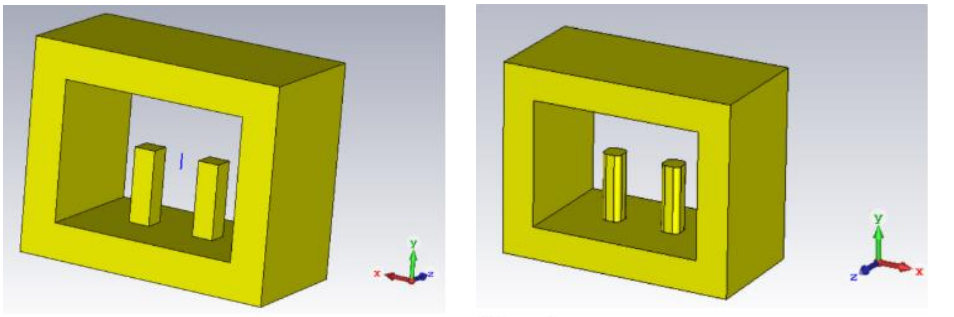


*Figure 1 Double corrugated waveguide without (a) and with fillet (b).*

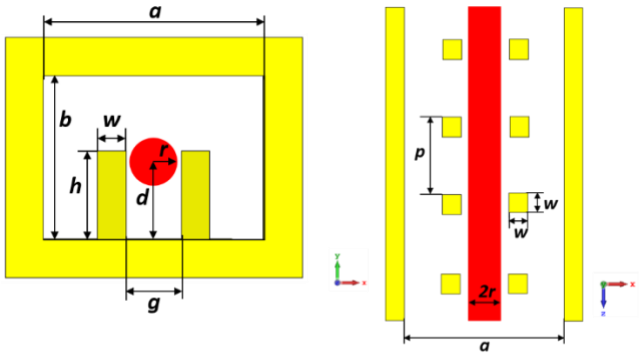


*Figure 2 Double corrugated waveguide schematic with dimensions.*

*Table 1 Nominal dimensions of the DCW*

| | |
|---|---|
| DCW width (a) | 800 μm |
| DCW height (b) | 588 μm |
| DCW period (p) | 550 μm |
| Pillar height (h) | 310 μm |
| Pillar width (w) | 90 μm |
| Beam radius (r) | 70 μm |
| Beam y position (d) | 280 μm |

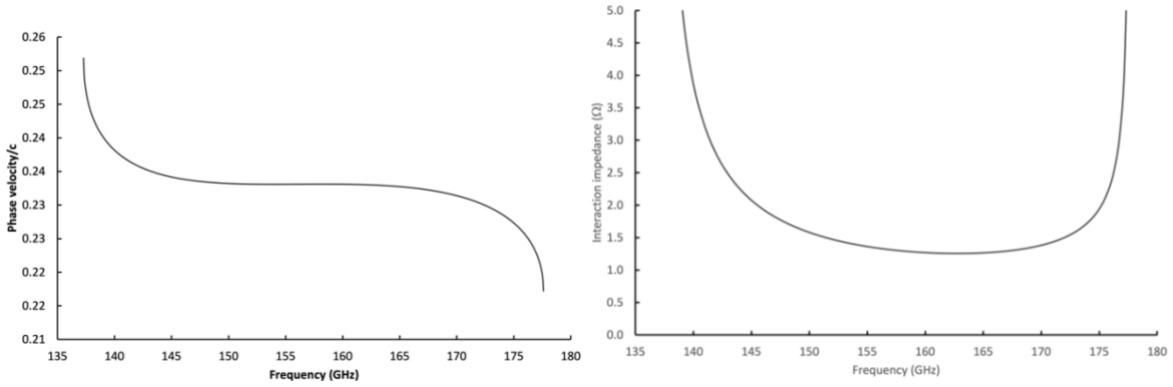


a) b)

*Figure 3 Normalized phase velocity (a) and Interaction impedance (b) in the frequency band 151 – 161.5 GHz.*

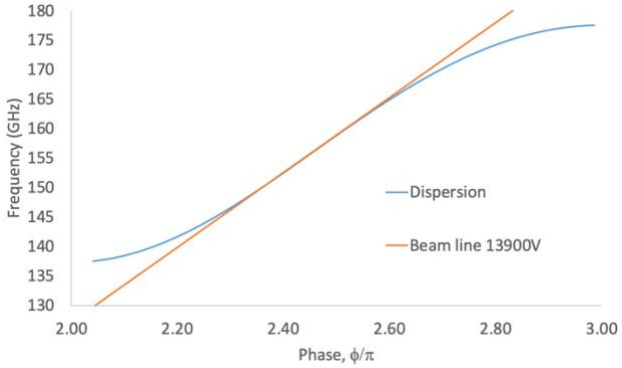


*Figure 4 Dispersion curve with beam line computed at 13900 V beam voltage.*

### 3. Double corrugated waveguide sensitivity analysis

Three most critical dimensions of the DCW are considered for the sensitivity analysis of dispersion and interaction impedance, specifically, height of the pillars *h*, DCW width *a* and period *p*. The position and the cross section of the electron beam are also important parameters for optimizing the performance. A specific sensitivity analysis to assess their impact on the interaction impedance will be also presented. In the following, all the dimensions are the nominal ones (Table 1), if not specified differently.

Figure 5 shows the effect of the variation of the height of the pillars *h* in the range 250 - 350 μm (nominal *h* = 310 μm). Fig. 5a shows a substantial shift of the dispersion curve and a variation of the phase velocity, decreasing at the increase of the pillar height *h* (both the lower cutoff frequency and upper stop band frequency decrease). The interaction impedance (Fig. 5b) increases at the increase of *h* with a variation higher than 50% the nominal value. To note the reduction in bandwidth. The variation of *h* has no specific impact on the operation center frequency.

Figure 6 shows the effect of the variation of the DCW width *a* in the range 800 -1000 μm (nominal *a* = 800 μm). Fig. 6a shows the increase of the dispersion at the increase of *a* (the lower cutoff frequency decreases, upper stop band frequency only slightly decreases), and a substantial increase decrease of flatness of the phase velocity with related reduction of the synchronism frequency band with the beam voltage. Fig. 6b shows a decrease of the interaction impedance at the increase of *a*. Fig. 6 demonstrates that the DCW width is very important for wide band behavior.

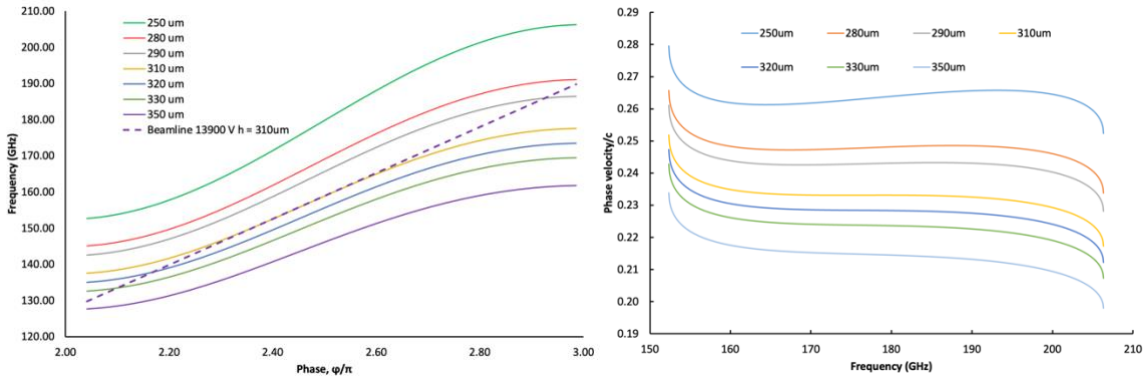


*a)*

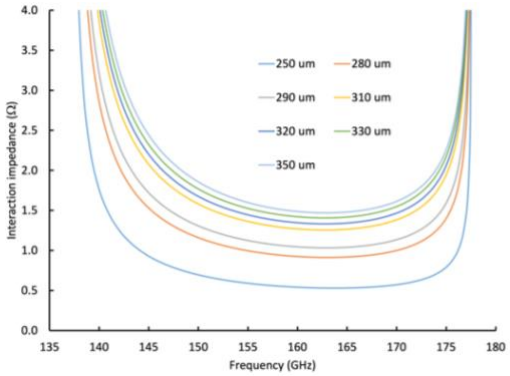


*b)*

*Figure 5 Dispersion curves (a) and interaction impedance (b) for pillar height 'h' variation.*

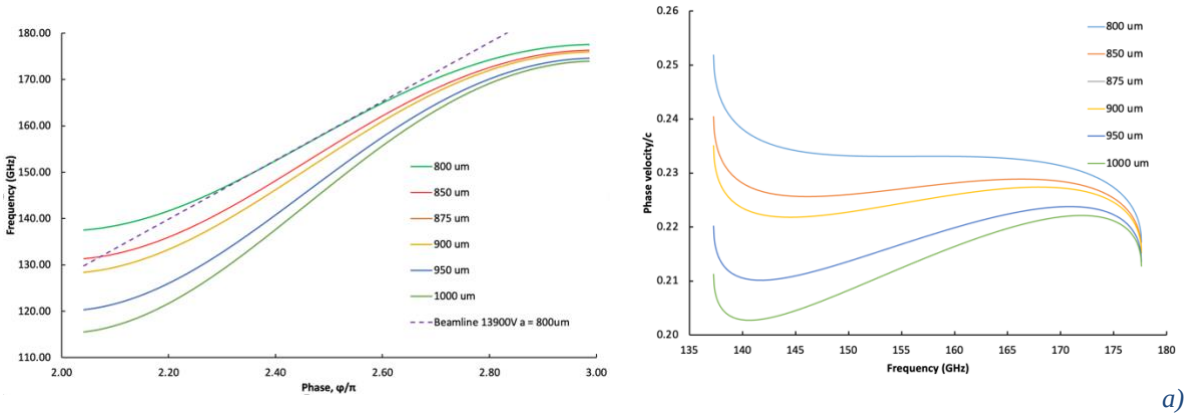


*a)*

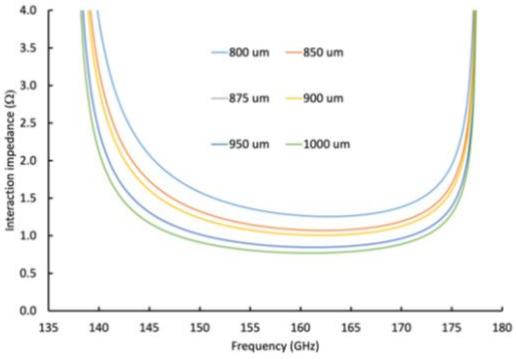


*b)*

*Figure 6 Dispersion curves (a) and interaction impedance (b) for waveguide width 'a' variation.*

Fig. 7 shows the sensitivity of dispersion to the DCW period *p*, varied in the range 550 - 750 μm (nominal 550 μm). Fig. 7a shows that at the increase of *p* the upper stop band frequency decreases substantially while the lower cutoff frequency has only a slight variation. The increase of the phase velocity at the increase of *p* is relevant. This is confirmed by the relation of *p* with the beam voltage $V_0$ for a given frequency *f* [12]:

$$p = \frac{\phi 5.93 * 10^5 \sqrt{V_0}}{2f} \tag{1}$$

where *f* is the frequency, $\phi$ is the phase shift.
To reduce the beam voltage, the period of the DCW has to be reduced, with possible fabrication constraints.
Fig. 7b shows that the interaction impedance increases at the increase of the period *p*. The accuracy of the period length is very important due to the substantial variations of dispersion and interaction impedance. To note that the dispersion remains flat, permitting, in case of variation an adjustment by varying the beam voltage.

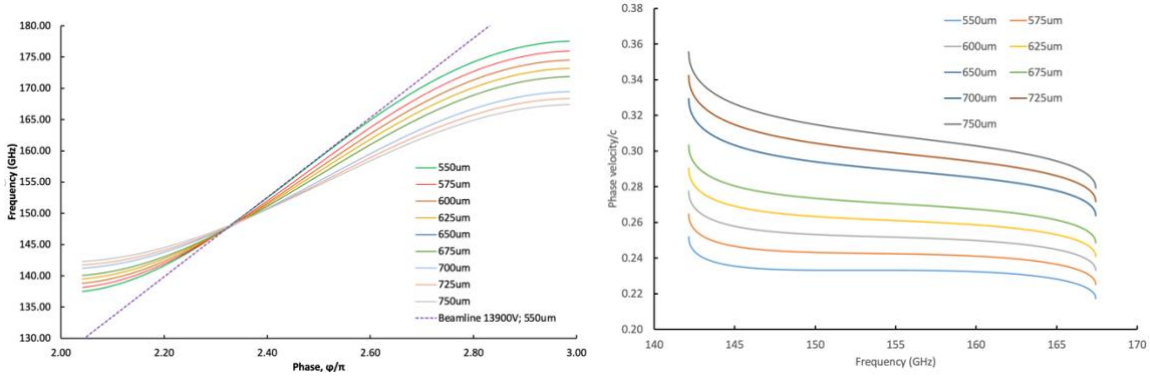


*a)*

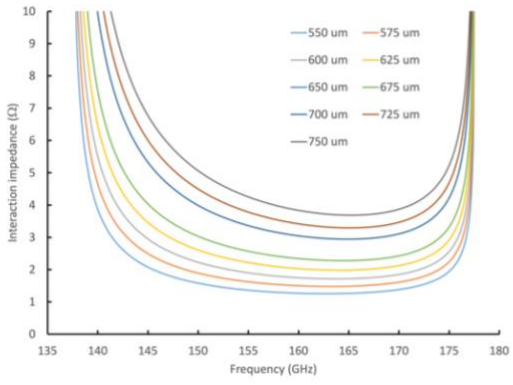


*b)*

*Figure 7 Dispersion curves (a) and interaction impedance (b) for period p variation*

The electron beam travels between the two rows of pillars, as shown in Fig.2. The horizontal position is fixed at the center of the two pillar rows. The vertical position of the beam center is set to expose the electron beam to the region where the electromagnetic field is more intense. The position of the electron beam has no effect on the dispersion, that will not be considered in the following.
Figure 8 shows the variation of the average interaction impedance computed on the beam cross section. As expected, the larger the area of the beam cross section and the proximity with the pillars increase the average interaction impedance.
Figure 9 shows the interaction impedance calculated at the center of the electron beam as a function of the vertical position *d* of the beam center, varied in the range 250 - 350 μm (nominal *d* = 280 μm). To note the region where the variation is minimum when the beam is close to the nominal position or lower. When the beam position is higher than the nominal position, the interaction impedance reduces due to the low electric field intensity. This behavior suggests that the position of the beam lower than the nominal one does not have a significant effect on the interaction impedance, making this dimension not very critical.

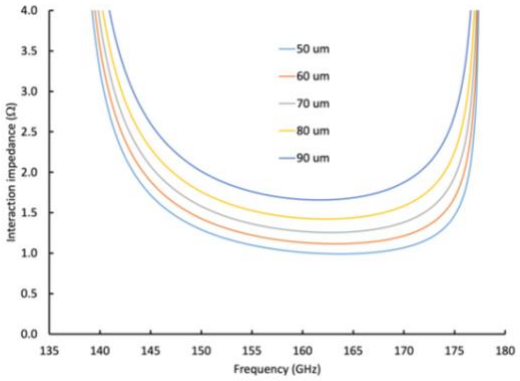


*Figure 8 Interaction impedance as a function of the beam radius (r) (cross section area).*

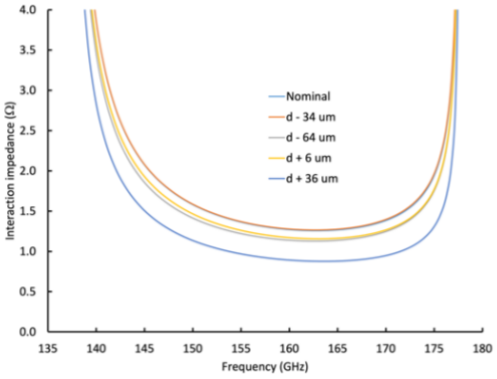


*Figure 9 Interaction impedance as a function of the electron beam center d computed as difference to the nominal position d = 280 μm.*

The graphs in Figs. 5 - 9 provide very useful general guidelines to design a DCW valid for any frequency band. Table 2 summarizes the direction of change of the various design parameters as a function of the variation of the main DCW dimensions. As an example, to increase the interaction impedance, the period should be longer, but at expense of the bandwidth. Obviously, to define the final dimensions of the DCW, it will be necessary to perform 3D electromagnetic simulations.

*Table 2 Effect of dimension variation on the DCW design parameters*

| **Parameter** | **DCW width *a*** | **Pillar period *p*** | **Pillar height *h*** | **Beam radius *r*** |
|---|---|---|---|---|
| **Dispersion** | Direct | Inverse | Inverse | - |
| **Bandwidth** | Direct | Inverse | Inverse | - |
| **Start frequency** | Inverse | Direct (slightly) | inverse | - |
| **Stop frequency** | Inverse (slightly) | inverse | Inverse | - |
| **Interaction impedance** | Inverse | Direct | Direct | Direct |
| **Beam voltage** | inverse | Direct | Inverse | - |

### 4. Sensitivity analysis as a function of fillet radius

Fillets may be introduced in the pillar geometry (Fig. 2b) either as a design approach to simplify the fabrication or due to eventual fabrication errors. Simulations were carried out to estimate the effect of fillets on dispersion, interaction impedance and beam voltage. The fillet radius ($r_f$) on pillar edges was varied in the range 0 (nominal value in case of sharp edges) - 25 μm. Figure 10 shows the presence of fillets determines a slight variation of the beam voltage and of

the dispersion that can easily compensate with a minor variation of beam voltage. To note the interaction impedance is not affected (Fig. 11). This study confirms the robustness of the DCW to variations of the shape of the pillars [13].

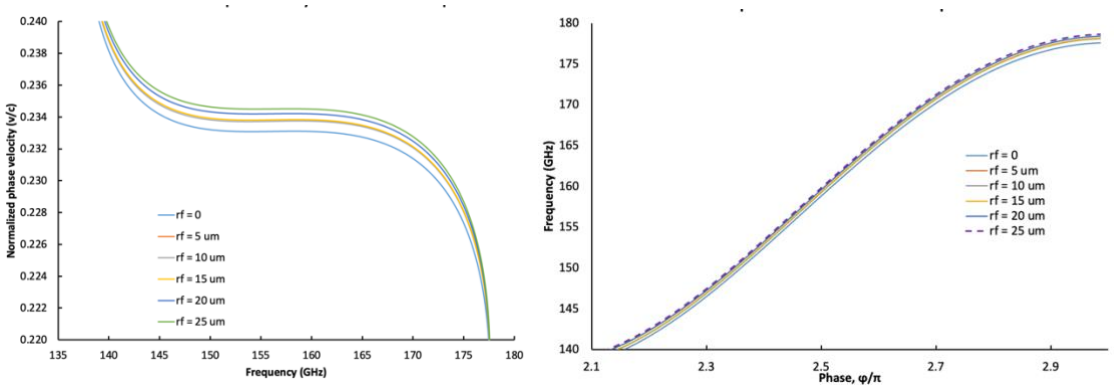


*Figure 10 Normalized phase velocity as a function of the fillet radius $r_f$.*

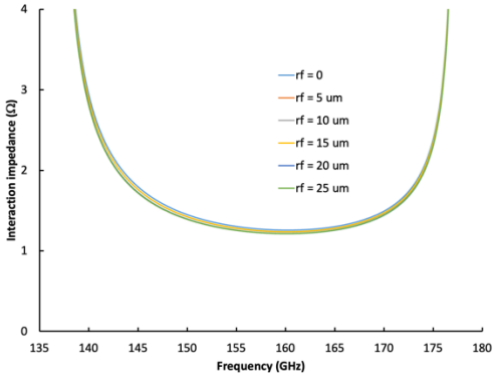


*Figure 11 Interaction impedance as a function of the fillet radius $r_f$.*

## 4. Conclusions

Sensitivity analysis of the geometry parameters is a powerful methodology to predict the deviation of the cold parameters from the nominal specifications and optimize the dimensions of the DCW. Due to the size of the computational domain, it is very difficult to do a sensitivity analysis by particle in cell simulations, but the information obtained by the sensitivity analysis of the cold parameters permits to predict possible improvement of performance and fabrication requirements. The study also highlights that some dimensions require different quality of the fabrication tolerance and permits to assess if eventual deviations could be corrected by tuning the beam voltage.
The presence of fillets in the pillars only slightly affects dispersion and interaction impedance, giving flexibility and allowing a margin of error for the pillar shape.


## Acknowledgement

The research described in this publication was made possible by the DLINK- D-band Wireless Link with Fibre Data Rate project funded by EPSRC grants EP/S009620/1.


## References


1. S. S. Dhillon and et. al., “The 2017 terahertz science and technology roadmap,” Journal of Physics D: Applied Physics, vol. 50, p. 043001, Jan 2017.
2. C. Paoloni, “Sub-THz wireless transport layer for ubiquitous high data rate,” IEEE Communications Magazine, vol. 59, no. 5, pp. 102–107, 2021.
3. T. Maiwald, T. Li, G.-R. Hotopan, K. Kolb, K. Disch, J. Potschka, A. Haag, M. Dietz, B. Debaillie, T. Zwick, K. Aufinger, D. Ferling, R. Weigel, and A. Visweswaran. A review of integrated systems and components for 6g wireless communication in the d-band. Proceedings of the IEEE, 111(3):220–256, 2023.

4. C. Paoloni, D. Gamzina, R. Letizia, Y. Zheng, and N. C. L. Jr., Millimeter wave traveling wave tubes for the 21st century. Journal of Electromagnetic Waves and Applications, 35(5):567–603, 2021.
5. D. Gamzina, L. G. Himes, R. Barchfeld, Y. Zheng, B. K. Popovic, C. Paoloni, E. Choi, and N. C. Luhmann. Nano-cnc machining of sub-THz vacuum electron devices. IEEE Transactions on Electron Devices, 63(10):4067–4073, 2016.
6. R. Basu, J. M. Rao, T. Le, R. Letizia, and C. Paoloni. Development of a D-band traveling wave tube for high data-rate wireless links. IEEE Transactions on Electron Devices, 68 (9):4675–4680, 2021.
7. F. Andre, J. Racamier, R. Zimmermann, Q. Trung Le, V. Krozer, G. Ulisse, D. F. G. Minenna, R. Letizia, and C. Paoloni, "Technology, assembly, and test of a W-band traveling wave tube for new 5g high- capacity networks," IEEE Transactions on Electron Devices, vol. 67, no. 7, pp. 2919–2924, 2020.
8. L. Wenqiang, J. Yi, Z. Quanfeng, H. Peng, H. Linlin, Y. Lei, and C. Hongbin, "Development of D-band continuous-wave folded waveguide traveling-wave tube," in 2015 IEEE International Vacuum Electronics Conference (IVEC), pp. 1–3, 2015.
9. Z. Wang et al., "Development of a 140-GHz folded-waveguide traveling-wave tube in a relatively larger circular electron beam tunnel," J. Electromagn. Waves Appl., vol. 31, no. 17, pp. 1914–1923, Nov. 2017.
10. M. Field, T. Kimura, J. Atkinson, D. Gamzina, N. C. Luhmann, B. Stockwell, T. J. Grant, Z. Griffith, R. Borwick, C. Hillman, B. Brar, T. Reed, M. Rodwell, Y.-M. Shin, L. R. Barnett, A. Baig, B. Popovic, C. Domier, R. Barchfield, J. Zhao, J. A. Higgins, and Y. Goren. Development of a 100-W 200-GHz high bandwidth mm-wave amplifier. IEEE Transactions on Electron Devices, 65(6):2122–2128, 2018.
11. Paoloni, C, Basu, R, Billa, L, Mahadev Rao, J, Letizia, R, Ni, Q, Wasige, E, Al-Khalidi, A, Wang, J & Morariu, R 2020, 'Long-range millimetre wave wireless links enabled by travelling wave tubes and resonant tunnelling diodes', IET Microwaves, Antennas and Propagation, vol. 14, no. 15, pp. 2110 - 2114. https://doi.org/10.1049/iet-map.2020.0084
12. M. Mineo and C. Paoloni. Double-corrugated rectangular waveguide slow-wave structure for terahertz vacuum devices. IEEE Transactions on Electron Devices, 57(11):3169–3175, 2010.
13. M. Mineo and C. Paoloni, "Improved corrugation cross-sectional shape in terahertz double corrugated waveguide," IEEE Transactions on Electron Devices, vol. 59, no. 11, pp. 3116–3119, 2012.